Effect of divalent transition metal ions on physical, morphological, electrical and electrochemical properties of alluaudite phases Na2M2+2Fe3+(PO4)3 (M = Mn, Co and Ni): Cathode materials for sodium-ions batteries

Douha Harbaoui, Moustafa M.S. Sanad, Cécile Rossignol, El Kebir Hlil, Noureddine Amdouni, Kader Zaidat, Saïd Obbade

Version of Record: https://www.sciencedirect.com/science/article/pii/S0925838822000329
Manuscript_d5cde9d2007ac71499b6e5e015adcdc9

Effect of Divalent Transition Metal Ions on Physical, Morphological, Electrical and Electrochemical Properties of Alluaudite Phases $Na_2M^{2+}{}_2Fe^{3+}(PO_4)_3$ (M = Mn, Co and Ni): Cathode Materials for Sodium-ions Batteries.

Douha Harbaoui[1-4], Moustafa M. S. Sanad[2], Cécile Rossignol[1], El Kebir Hlil[3], Noureddine Amdouni[4], Kader Zaidat[5] and Saïd Obbade[1]

[1] *Univ. Grenoble Alpes, Univ. Savoie Mont Blanc, CNRS, Grenoble INP**, LEPMI, 38000 Grenoble, France.*
[**] *Institute of Engineering and Management Univ. Grenoble Alpes*

[2] *Chemical & Electrometallurgy Department, Central Metallurgical R & D Institute, P.O. Box 87 Helwan, Cairo, Egypt*

[3] *Université Grenoble Alpes, CNRS, Grenoble INP, Institut Néel, BP 166, F-38042 Grenoble cedex 9*

[4] *Université El Manar, U.R. Physico-Chimie des Matériaux Solides, 1060 Tunis, Tunisie*

[5] *Univ. Grenoble Alpes, Grenoble-INP, CNRS, SIMaP, F-38000 Grenoble, France*

Abstract

The limited resources of lithium stimulated the research work to develop new polyanionic cathode materials for sodium-ion batteries. The $Na_2M^{2+}{}_2Fe^{3+}(PO_4)_3$ (M = Mn, Ni and Co) phases were prepared by autocombustion method assisted by glycine. Structural, morphology, thermal, electrical and electrochemical properties have been investigated. Its structures were determined using Xray powder diffraction and Rietveld method refinements. The two compounds $Na_2M^{2+}{}_2Fe^{3+}(PO_4)_3$ (M = Mn and Co) are alluaudite-type. Both compounds crystallize in monoclinic system with the space group C2/c and similar parameters: a= 12.0337(3) Å, b= 12.6268(3) Å, c= 6.5070(1) Å, β=114.563(2)° for $Na_2M^{2+}{}_2Fe^{3+}(PO_4)_3$ (NMFP) and a= 11.7597(3) Å, b= 12.4579(3) Å, c= 6.4607(1) Å, β=113.968(1)° for $Na_2Co_2Fe(PO_4)_3$ (NCFP). The $NaNiFe_2(PO_4)_3$ (NNFP) compounds crystallize in orthorhombic system with the space group Imma and unit cell parameters: a= 10.3993(1) Å, b= 13.1966(1) Å, c= 6.4955(1) Å. The composition and morphology of the compounds were checked by energy dispersive spectroscopy coupled with scanning electron microscope. The thermal analysis confirmed the allotropic transition of the three materials from monoclinic to orthorhombic symmetry with the changing of divalent transitions metal ion. The electrical conductivity results of indicated that NNFP has the lowest value of activation energy of value= 0.63 eV owing to the large size of open channels existed in the orthorhombic symmetry. The electrochemical cycling results showed that NMFP cathode delivered the maximum storage capacity of about 94.2 mAh/g which correspond to coloumbic efficiency of about 75.5 % after the initial cycling.

Keywords: Structure refinement, Surface morphology, Transition metals, Ionic conductivity, Charge-discharge profile

****corresponding authors:*** ***said.obbade@phelma.grenoble-inp.fr***

1. Introduction

Due to the huge incremental demand of electric and hybrid vehicles in the world, the battery market is rapidly growing and expanding in few years. Therefore, the implementation of the electrochemical energy storage devices such as lithium-ion batteries has attracted much interest in the transport and the urban mobility field, such as hybrid electric vehicles (HEVs), plug-in hybrid electric vehicles (PHEVs), and electric vehicles (EVs) [1-3]. However, the commercial expansion of such technology is potentially restricted by the limited resources of Li metal [4, 5]. To overcome this barrier, Sodium-Ion Batteries (SIBs) have emerged as a promising candidate, where sodium metal offers good standard reduction potential ($E°$=-2.71 V vs "Standard Hydrogen Electrode" for the Na^+/Na) and large abundance in the earth-crust (in 6th rank with 23600 ppm) [6-11]. Thus, such technology is a promising option for large scale applications in which cost and safety more than energy density is a primary factor. Faced with this global energy demand which has continued to increase in recent decades, with energy production that will have to keep up with the frantic pace of population growth, and an excessive energy consumption leading to a rapid worsening of environmental problems, it seems necessary and imperative to develop new Na-ion technology accumulators. For this, it is therefore necessary to explore and propose new phases that could be used such as sodium ion insertion materials, which are electrochemically reversible, with a lifetime competitive with lithium-ion technology systems. These new needs have therefore stimulated the research teams to search materials with new structures suitable for the electrochemical insertion of sodium. As a result, various positive electrode materials have been reported for Na-ion technology batteries, such as transition metal oxides adapting layered structures [12-16], transition metal sulfides and fluorides [17-21], polyanionic compounds [22-31], Prussian blue analogs, organic carboxylates and polymers [32-35].

Recently, new polyanionic sodium compounds have been identified and then tested as positive electrodes in SIBs [36, 37]. Likewise, a number of iron or vanadium polyphosphate compounds have been also considered as an electropositive materials for Na-ions Batteries [38-41].

Mixed sodium transition metal polyphosphates with an alluaudite framework structure, of monoclinic symmetry and space group C2/c, are also known with the possibility of containing bi and/or trivalent transition metals, [42-47]. It has been also observed that the presence of mixed transition elements could enhance the intrinsic ionic conductivity and improve the redox potential of polyanionic compounds which positively reflects on sodium ions intercalation through the tunnels in the crystal structure [48, 52]. Indeed, the alluaudite phaes, with general formula $A(1)A(2)M_2(1)M(2)(PO_4)_3$ where A sites are may bee occupied by a large monovalent and/or divalent cations number (Na^+, K^+, Ca^{2+} …) in eight-coordination and where the M sites occupied by transition metal cations in octahedral environment [53]; exhibit an open structure, in which there is a

succession of monodimensional channels occupied by A cations . The presence of A cations in these large channels confer them a large ionic mobility in such a structure, that gives rise to interesting electrical conductivity. The presence of vacancies at A sites in such an open structural framework facilitates the intercalation/desintercalation of alkali ions in these alluaudites, classifying them amidst promising polyanionic positive-electrode materials for secondary batteries [54, 55]. Besides promising electrochemical activities, the capcity of alluaudite-like structures to accommodate a wide selection of transition metals can also confer them additional attractive features like electronic and/or ionic conductivity, magnetism, catalytic activity; in addition, iron-phosphate-based alluaudite shows high thermal stability [42, 49, 56, 57].

Thus, different research groups have recently reported diverse Allaudite-type compounds in the formula $Na_2M^{2+}{}_2Fe^{3+}(PO_4)_3$ with Ni^{2+}/Fe^{3+} mixed elements that could be stabilized in the orthorhombic crystal structure with Imma space group and polyanionic framework more symmetric [50]. Moreover, other recent study confirmed that the presence of Ni^{2+}/Cr^{3+} and Ni^{2+}/Al^{3+} in polyphosphate allaudite-type compounds favor also the crystallization as orthorhombic crystal structure [51, 52].

In this context, this work is focused on synthesis of new sodium phosphate phases-type $Na_2M^{2+}{}_2Fe^{3+}(PO_4)_3$, contining different divalent chemical elements (M = Mn, Co and Ni), to get mixed transition metal cations (Mn^{2+}/Fe^{3+}, Co^{2+}/Fe^{3+} and Ni^{2+}/Fe^{3+}) and investigate suitable sodium host materials with high redox potential for Na-ion batteries (SIBs). In addition, the present study aims at understanding the link between crystal structure and electrical behavior of these compounds.The thermal stability and morphological aspects of the as-prepared compounds are an area of ineterest. Finally, the influence of different divalent cations on the electrical conductivity and electrochemical performance as positive electrodes are presented.

2. Experimental

Different samples of general formula $Na_2M^{2+}{}_2Fe^{3+}(PO_4)_3$, where M = Mn, Co, Ni, were synthesized by auto-combustion method. The nitrate and acetate salts act as oxidizers, while glycine acts as the fuel and complexing agent. As indicated in figure 1, for preparation of monoclinic precursors NMFP and NCFP, stoichiometric amounts of $Mn(COOCH_3)_2{\cdot}4H_2O$ (Prolabo 99.9%) or $Co(NO_3)_2{\cdot}6H_2O$ (Acros 100 %) were used, while $Ni(NO_3)_2{\cdot}6H_2O$ (Acros 99.99 %) was used as source of Ni^{2+} ions for preparation of monoclinic precursors NNFP. The previous salts were subsequently dissolved with corresponding proportions of $NaNO_3$ (Alfa-Aesar 98.9%) and $Fe(NO_3)_3{\cdot}9H_2O$ (Sigma-Aldrich 99.9%) in 0.4 M of glycine solution $C_2H_5NO_2$ (Alfa-Aesar 99%). The required amount of $NH_4H_2PO_4$ (Acros 99.9%) was added to the first mixture and stirred for 30 mn. The resultant solution mixture was heated at 120°C to evaporate the excess water and obtain

viscous foams that subsequently auto-ignited producing fine particles of colored precursors. The dried precusors were fired in a muffle furnace through two calcination steps. The first step involves heating all samples at 400 °C for 5h in order to remove carbon and nitrogen residues. The fired samples of NMFP and NCFP were successively ground and calcined at 750 °C for 48h, yielding dark violet and blue powders for $Na_2Mn^{2+}{}_2Fe^{3+}(PO_4)_3$ and $Na_2Co^{2+}{}_2Fe^{3+}(PO_4)_3$, respectively. The fired precursor of NNFP sample were also calcined at 850 °C for 48h to obtain yellow $Na_2Ni_2Fe(PO_4)_3$ powders. All the obtained powders were subsequently ground to be ready for further characterizations.

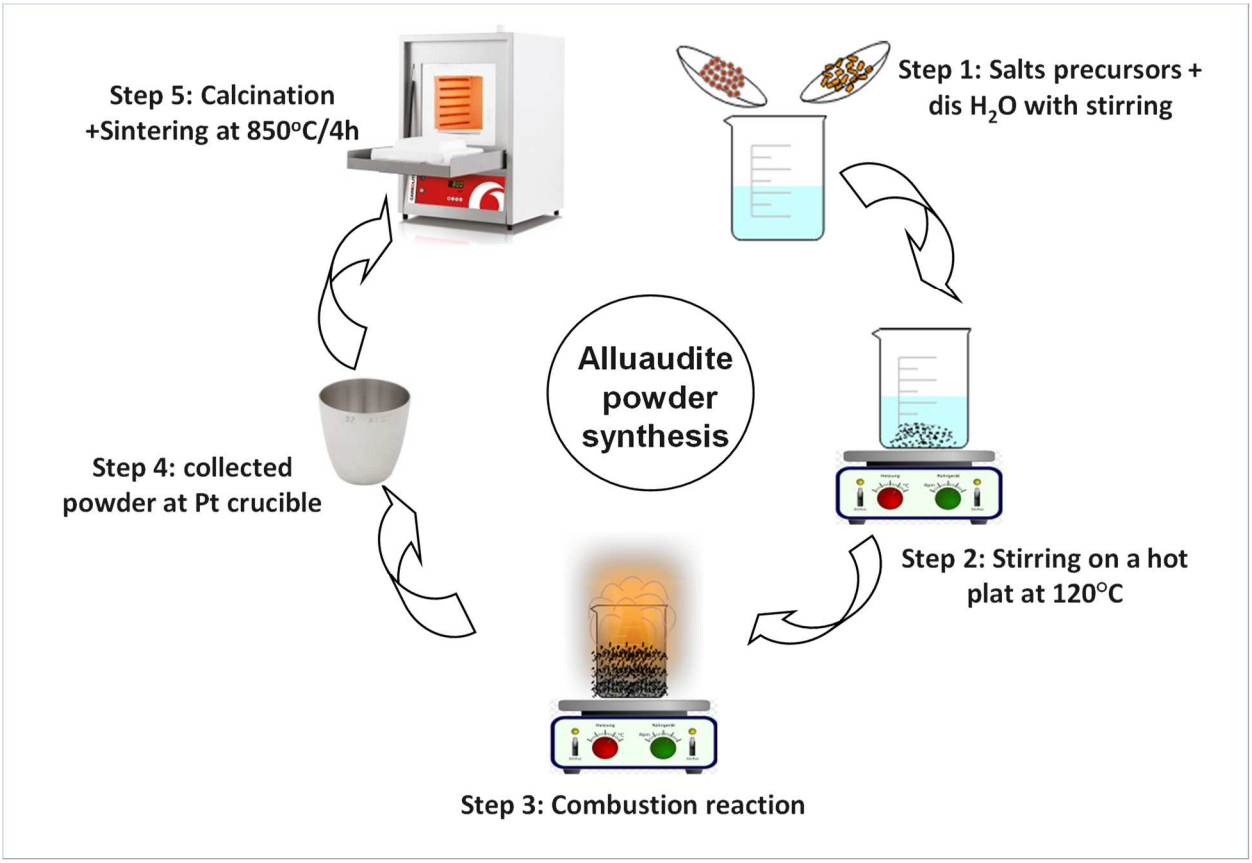

Figure 1. Synthetic procedure of Alluaudite powders

Powder X-ray diffraction data have been collected with an X'pert PRO PANalytical θ/2θ diffractometer equipped by CuKα radiation, using Bragg-Brentano geometry, in steps of 0.02°. The counting time is 40s per step, within an angular range of 10 to 90° in 2θ. For pure phases, Rietveld method has been used for crystal structure refinement, using powder X-ray diffraction data.

Surface morphology and elemental analysis were examined by field emission gun-scanning electron microscope (FEG-SEM) Carl ZEISS–model ULTRA 55 equipped with microanalysis BRUKER AXS, detector SDD 30 mm^2 and Energy Dispersive X-ray Spectroscopy analyzer (EDS).

Thermal analyses (TG/DTA) were performed under air flow (20 ml/min), using a SETARAM TAG24-16 thermal analyzer, and platinum crucibles. For each sample thermal measurements were carried out in the range of room temperature to 800 °C, with fixed heating rate 5°C.min^{-1} and all the DTA curves were normalized with respect to the sample weight.

Electrical conductivity measurements, by Impedance spectroscopy technique, were carried out on the gold coated pellets, using SC7620 Mini-sputter coater. The impedance diagrams were recorded with an applied voltage of 50 mV from 300 to 650 °C and under zero dc conditions in the 5Hz to 13MHz frequency range, using Hewlett-Packard frequency response analyzer (4192 ALF). The sample densities were measured from the size and weight of sintered pellets.

For the electrochemical measurements, the carbon coating of the pure phase powders were carried out by mixing sucrose with certain amount corresponding to 10% C using ball mill and then, calcined at 650 °C under inert atmospheric conditions.

For electrochemical measurements, the used positive electrodes have been prepared by mixing 80 wt% of $Na_2M^{2+}{}_2Fe^{3+}(PO_4)_3$ (M = Mn, Co, Ni) active material, 10 wt% of Super P carbon, and 10 wt% of the polyvinylidene fluoride (PVDF) as binder dissolved in N-methylpyrrolidone (NMP) solution. For each compound, the formed homogenous mixture was coated on aluminum foil using screen printing technique, and then dried at 70°C under vacuum. The electrochemical tests were carried out using coin cells (CR2025) assembled in Ar-filled glove box. The average mass loading of the active material was around 3 mg/cm^2 and Na metal foil acts as the negative electrode with Celgard 2400 as the separator. The cell electrolyte was 1M $NaClO_4$ in propylene carbonate (PC). Galvanostatic charge-discharge cycling and EIS measurements for the assembled batteries were conducted in the potential range of 1.5–4.2 V (vs. Na^+/Na) under various current densities using VMP-300 multipotentiostat (BioLogic SAS) where the 1C rate =0.2 mA/g.

3. Results and discussion

3. 1. Crystal structures determination and description

The crystal structures refinement of the different phases were carried out by the Rietveld option of Fullprof program, [58- 60], using X-ray diffraction data. The final results of the Rietveld refinement of the diffractograms of the monoclinic (NMFP, NCFP) and orthorhombic (NNFP) phases are shown in Figures 2 (2a, 2b) and 3, respectively. The crystallographic data and the detail of the refinements for the three compounds are collected in Table 1. The atomic positions and the isotropic thermal stirring coefficients for the three compounds are presented in Table 2 and 3. The interatomic distances are collated in Tables 4 and 5.

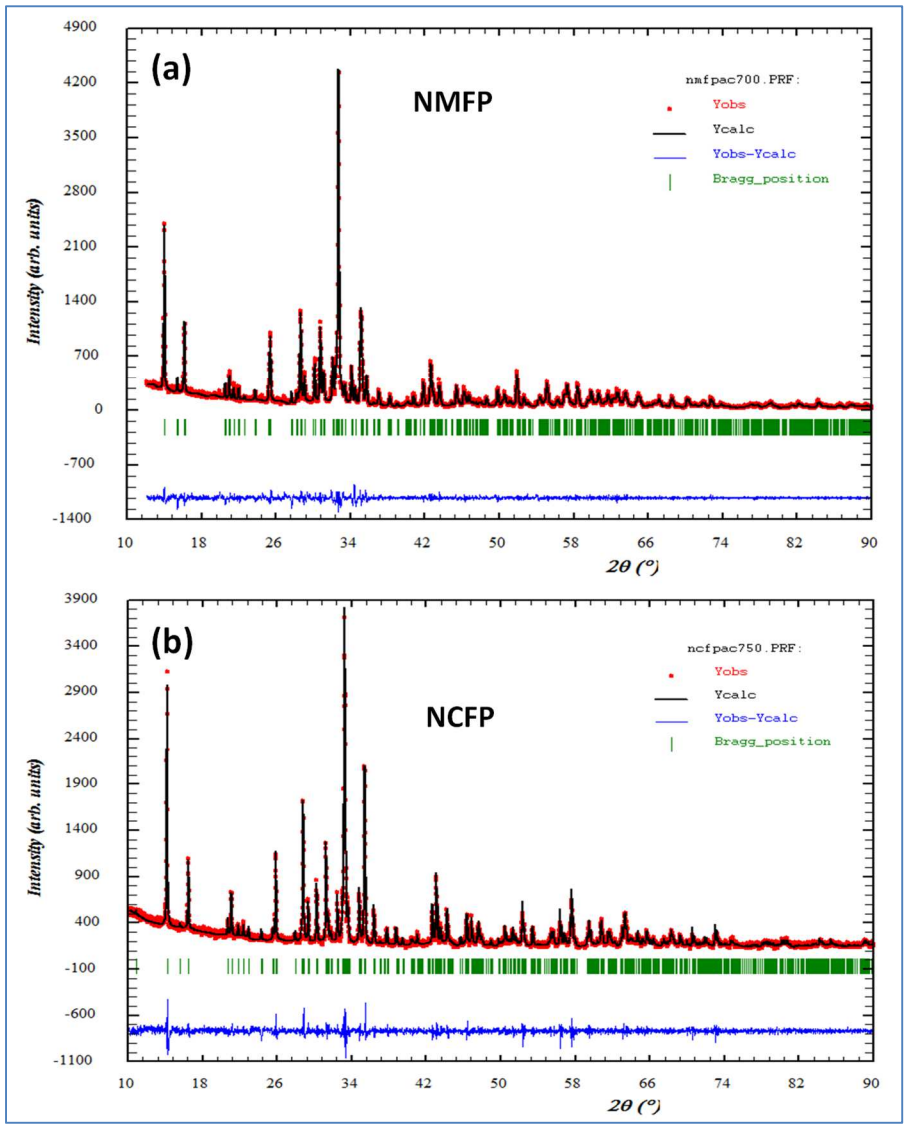

Figure 2. Diffractograms of the observed (red), calculated (black) and a difference between the two (blue) patterns for monoclinic compounds, (a) NMFP, (b) and NCFP.

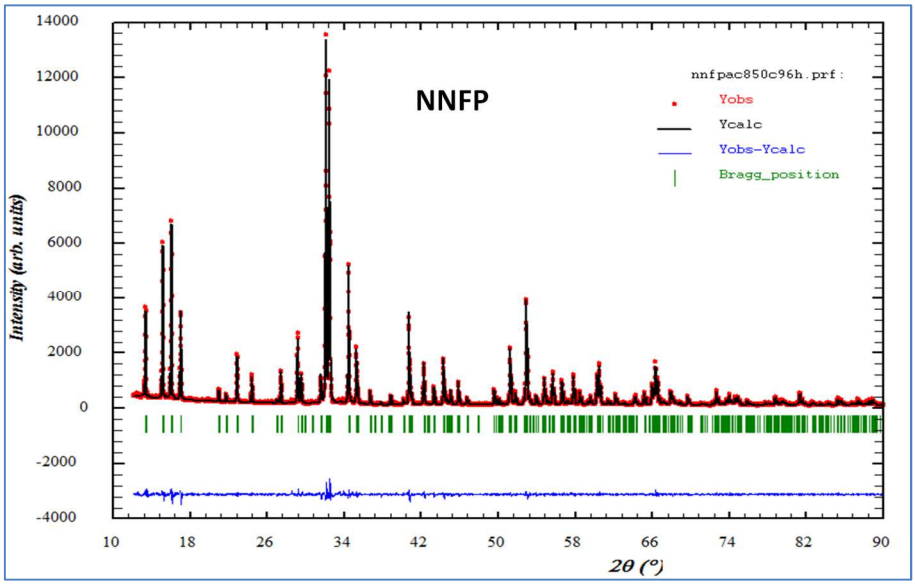

Figure 3. Diffractograms of the observed (red), calculated (black) and a difference between the two (blue) patterns for the orthorhombic compounds, NNFP.

Table 1. Structures refinement details for NMFP, NCFP and NNFP phases.

Crystal data			
Chemical formula	**NMFP**	**NCFP**	**NNFP**
M_r	504.61	496.61	475.26
Crystal system, space group	Monoclinic ; C2/c		Orthorhombic ; Imma
Unit cell dimensions (Å, °)	a= 12.0337(3), b= 12.6268(3), c= 6.5070(1), β=114.563(2)	a= 11.7597(3), b= 12.4579(3), c= 6.4607(1), β=113.968(1)	a= 10.3993(1), b= 13.1966(1), c= 6.4955(1)
V* (Å^3) ; *Z	899.24(5) ; 4	945.99(1) ; 4	891.35(2) ; 4
Data collection			
Diffractometer	Panalytical		
Wavelength (Å)	CuK(α1,α2)		
Temperature (K)	300		
2θ values	10 - 91	10 - 91	10 - 91
Counting time	0.016° / 40 s		0.016° / 40 s
Refinement			
Rp	0.045	0.086	0.035
Rwp	0.064	0.099	0.047
Rexp	0.051	0.080	0.010
R(F²)	0.026	0.049	0.031
RBragg	0.034	0.044	0.034
Numberof parameters	114	114	104
Profile function	Pseudo-Voigt		

Table 2. Atomic coordinates and Biso isotropic displacement factors of the monoclinic structures of NMFP, M = Mn, Co.

Name	Sites	x	y	z	B_{iso}
$Na_2Mn_2Fe(PO_4)_3$					
Na(1)	*4a*	1/2	1/2	0	3.93(25)
Na(2)	*4e*	0.0000	0.4829(1)	3/4	4.61(40)
Co	*8f*	0.7232(5)	0.8445(3)	0.1409(7)	1.64(10)
Fe	*4e*	1/2	0.7315(5)	3/4	3.61(7)
P(1)	*8f*	0.7635(7)	0.6068(5)	0.3747(2)	2.25(19)
P(2)	*4e*	1/2	0.2876(7)	1/4	1.20(23)
O(1)	*8f*	0.7729(10)	0.6733(10)	0.1780(20)	1.84(36)
O(2)	*8f*	0.8315(13)	0.6645(11)	0.5970(20)	2.66(37)
O(3)	*8f*	0.8276(10)	0.5001(11)	0.3843(18)	1.96(34)
O(4)	*8f*	0.6283(11)	0.5957(8)	0.3255(20)	1.21(38)
O(5)	*8f*	0.6071(14)	0.3654(9)	0.2340(20)	2.90(35)
O(6)	*8f*	0.4535(11)	0.2217(10)	0.0370(20)	0.90(34)
$Na_2Co_2Fe(PO_4)_3$					
Na(1)	*4a*	1/2	1/2	0	3.44(32)
Na(2)	*4e*	0.0000	0.4832(1)	3/4	3.10(37)
Co	*8f*	0.7183(5)	0.8427(3)	0.1331(8)	2.23(12)
Fe	*4e*	1/2	0.7324(5)	3/4	3.45(721)
P(1)	*8f*	0.7644(7)	0.6094(6)	0.3758(2)	2.90(22)
P(2)	*4e*	1/2	0.2910(9)	1/4	2.80(31)
O(1)	*8f*	0.7809(11)	0.6783(10)	0.1880(20)	1.65(43)
O(2)	*8f*	0.8408(14)	0.6633(11)	0.6060(20)	3.30(42)
O(3)	*8f*	0.8313(8)	0.5013(11)	0.3885(17)	0.25(33)
O(4)	*8f*	0.6268(13)	0.5973(9)	0.3300(20)	1.60(44)
O(5)	*8f*	0.6071(14)	0.3665(9)	0.2550(20)	1.54(40)
O(6)	*8f*	0.4578(12)	0.2218(11)	0.0330(20)	1.99(43)

Table 3. Atomic coordinates and Biso isotropic displacement factors of the orthorhombic structures of NNFP

	Sites	x	y	z	B_{iso}
$Na_2Mn_2Fe(PO_4)_3$					
Na(1)	*4e*	0	3/4	0.6091(8)	4.61(19)
Na(2)	*4b*	0	1/2	1/2	4.14(20)
Ni	*8g*	1/4	0.6368(1)	1/4	1.05(4)
Fe	*4a*	1/2	1/2	1/2	1.08(7)
P(1)	*8g*	1/4	0.4282(2)	1/4	0.989(71)
P(2)	*4e*	0	3/4	0.0865(6)	1.05(10)
O(1)	*16j*	0.2892(3)	0.3676(3)	0.0632(4)	0.73(10)
O(2)	*16j*	0.1382(3)	0.5070(3)	0.2105(5)	0.71(11)
O(3)	*8h*	0	0.6547(4)	0.9527(2)	0.84(14)
O(4)	8i	0.1200(5)	3/4	0.2268(3)	0.56(15)

Table 4. Interatomic distances (Å) for NMFP, M = Mn and Co.

Distances	***$Na_2Mn_2Fe(PO_4)_3$***		***$Na_2Co_2Fe(PO_4)_3$***	
Na(1)–O(5) (×2)	2.248(11)		2.320(11)	
Na(1)–O(4) (×2)	2.369(10)		2.378(11)	
Na(1)–O(4) (×2)	2.567(15)		2.496(12)	
Na(1)–O(5) (×2)	2.964(16)	**<2.537>**	2.912(15)	**<2.526>**
Na(2)–O(3) (×2)	2.431(10)		2.383(10)	
Na(2)–O(3) (×2)	2.573(14)		2.493(11)	
Na(2)–O(2) (×2)	2.762(17)		2.826(12)	
Na(2)–O(6) (×2)	2.947(17)	**<2.678>**	2.858(10)	**<2.640>**
Fe–O(2) (×2)	2.221(12)		2.155(15)	
Fe–O(6) (×2)	2.269(14)		2.157(15)	
Fe–O(4) (×2)	2.277(15)	**<2.256>**	2.167(14)	**<2.160>**
M–O(2) (×1)	2.023(17)		1.903(16)	
M–O(2) (×1)	2.044(14)		2.049(14)	
M–O(6) (×1)	2.071(17)		2.069(13)	
M–O(6) (×1)	2.078(13)		2.069(17)	
M–O(4) (×1)	2.107(10)		2.095(15)	
M–O(4) (×1)	2.229(13)	**<2.092>**	2.156(14)	**<2.057>**
P(1)–O(4) (×1)	1.528(16)		1.530(17)	
P(1)–O(2) (×1)	1.519(14)		1.544(14)	
P(1)–O(3) (×1)	1.541(15)		1.545(15)	
P(1)–O(1) (×1)	1.574(17)	**<1.541>**	1.561(15)	**<1.545>**
P(2)–O(6) (×2)	1.532(17)		1.546(14)	
P(2)–O(5) (×2)	1.584(13)	**<1.558>**	1.562(17)	**<1.554>**

Table 5. Interatomic distances (Å) for NFP.

Distances	***$Na_2Ni_2Fe(PO_4)_3$***	
Na(1)–O(3) (×2)	2.626(9)	
Na(1)–O(1) (×4)	2.702(5)	
Na(1)–O(4) (×2)	2.783(8)	**<2.704>**
Na(2)–O(2) (×4)	2.369(5)	
Na(2)–O(1) (×4	2.833(4)	**<2.612>**
Ni–O(4) (×2)	2.021(5)	
Ni–O(2) (×2)	2.076(4)	
Ni–O(1) (×2)	2.086(3)	**<2.061>**
M–O(2) (×4)	1.986(6)	
M–O(3) (×2)	1.934(7)	**<1.968>**
P(1)–O(1) (×2)	1.509(4)	
P(1)–O(2) (×2	1.581(5)	**<1.545>**
P(2)–O(3) (×2)	1.543(7)	
P(2)–O(4) (×2)	1.640(7)	
Ni─Ni	2.8987(2)	**<1.594>**

For the two compounds NMFP and NCFP with monoclinic symmetry, the refinement of the crystal structure, from the X-ray powder diffraction data, was carried out by means of the Rietveld method in space group C2/c, using the model adopted by Khiem Trad et al. [43]. The refinement of the structural and profile parameters of NMFP and NCFP phases was continued until convergence of the different factors of reliability, R_{Bragg}, R_F, Rp and R_{wp}, as previously presented in **Table 1**. The diffraction diagrams presented in **Figure 2** reveal the agreement between the observed and calculated diffractograms. The low values of the reliability factors obtained at the end of the refinements also attest to the quality of the structural determination.

In the monoclinic structure of NMFP and NCFP compounds, the bivalent M^{2+} (M =Mn or Co) and trivalent Fe^{3+} metal atoms occupy the crystallographic sites 8f and 4e, respectively, where they adopt two deformed octahedral environments MO_6 and FeO_6, **Table 4**. The two independent atoms of phosphorus P1 and P2 adopt an environment tetrahedral, in fully occupied 8f and 4e sites, with mean distances <P1–O> ranging from 1.541 to 1.545 Å and <P2-O> ranging from 1.558 to 1.544 Å, in NMFP and NCFP, respectively. In the two isotype structures, each FeO_6 octahedron, associates with two MO_6 octahedra, sharing the opposite sides O2–O6 to form an anionic $[(MO_6)(FeO_2)MO_6]^{21-}$ $[(MO_6)(FeO_2)MO_6]^{21-}$ trimer, where each trimeric entity $[(MO_6)(FeO_2)MO_6]^{21-}$ is connected from both adjacent sides by the O1–O1 edges of the MO_6 octahedra, with two other $[(MO_6)(FeO_2)MO_6]^{21-}$ trimer, to form an infinite $^1_\infty[FeM_2O_{12}]^{17-}$ chain in the plane (a, c), as shown in **Figure 4.**

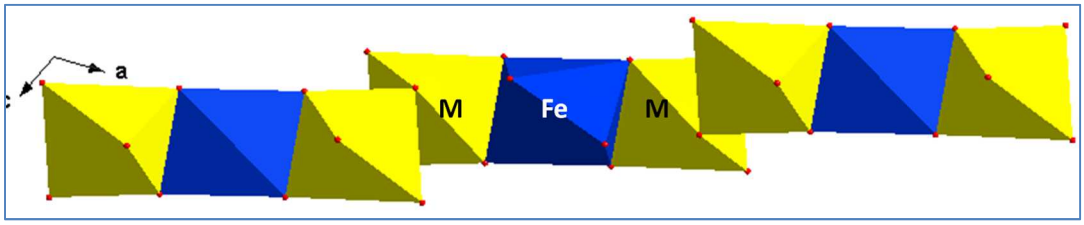

Figure 4. Infinite chain $^1_\infty[FeM_2O_{14}]^{21-}$ in the structure of compounds NMFP (M = Mn, Co).

The infinite $^1_\infty[FeM_2O_{12}]^{17-}$ chains are linked together by the intermediary of the tetrahedra PO_6 of the two phosphorus atoms P1 and P2, to constitute an infinite anionic layer $^2_\infty[FeM_2P_3O_{14}]^{6-}$ parallel to the (010) plane, like c 'is shown in **Figure 5**.

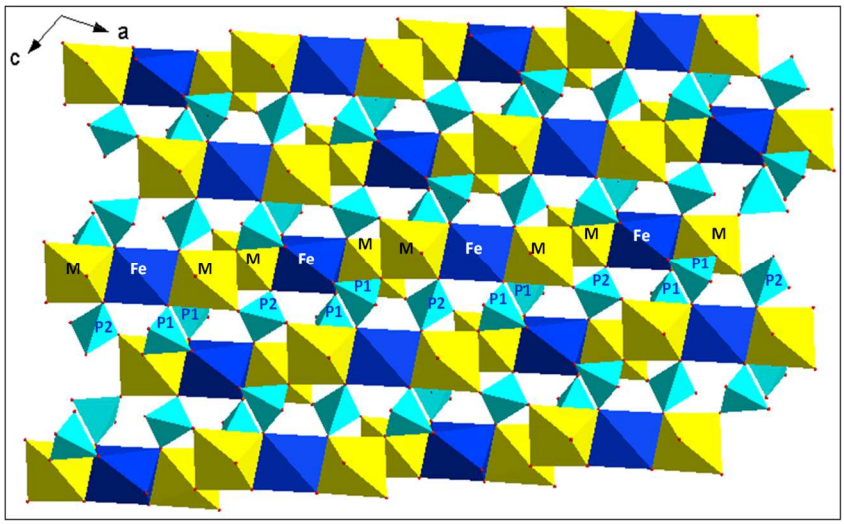

Figure 5. View of infinite layer $^{2}_{\infty}[FeM_2P_3O_{14}]^{6-}$ parallel to the (010) plane, in the structure of compounds NMFP (M = Mn, Co).

Thus, the crystal structure of both compounds NMFP and NCFP, is obtained by a stacking along the axis [010], infinite layers $^{2}_{\infty}[FeM_2P_3O_{14}]^{6-}$, linked together by the pooling oxygen atoms O3 between two consecutive layers; connecting the PO_4 tetrahedra of the phosphorus P1 atoms and the MO_6 octahedra of the bivalent metal to form a three-dimensional anionic framework $[FeM_2(PO_4)_3]^{2-}$, releasing two types of hexagonal tunnels, parallel to the axis [001] and occupied in an alternating manner by the sodium atoms Na1 and Na2. Thus, the monovalent Na^+ counter cations are located at the centers of the tunnels and participate in the cohesion of the structure, **Figure 6.**

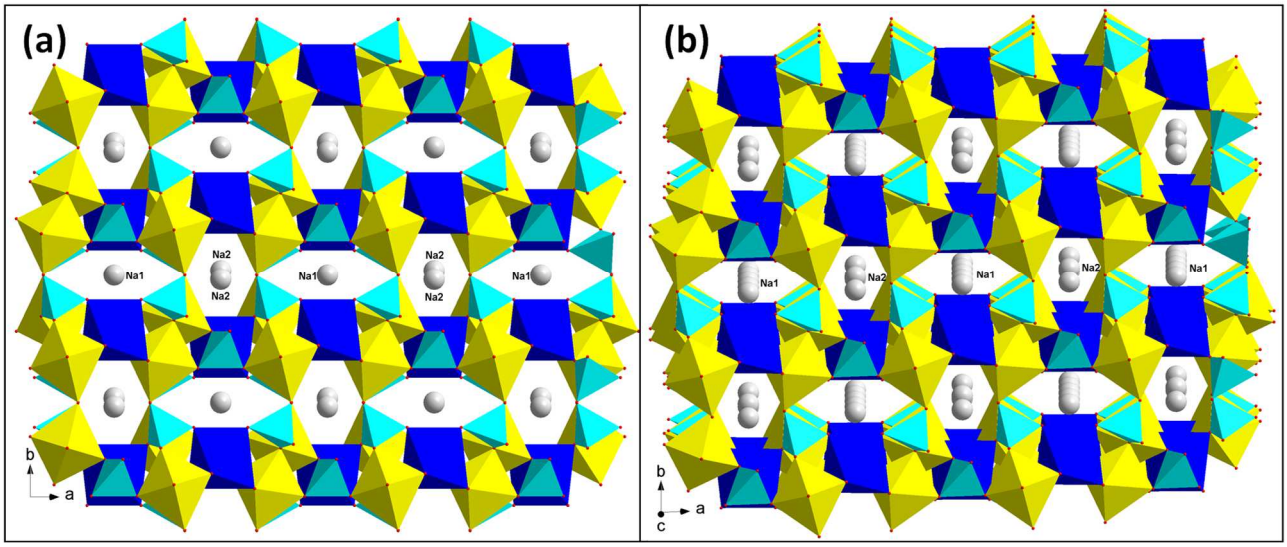

Figure 6. Projection views of the crystal structure of NMFP (M = Mn, Co), along: (a) axis [001] and (b) slightly deviated from direction [001].

Inside each chanal occupied by the alkaline cations Na1, the oxygen atoms O4 and O5 common to all the polyhedra MO_6, FeO_6 and PO_4, form deformed parallelepipeds O(4)O(4)O(5)O(5)─O(5)O(5)O(4)O(4) around the Na1 atoms; connected to each other alternately by one of the two rectangular faces O(4)O(4)O(5)O(5) and O(5)O(5)O(4)O(4) (**Figure 7**).

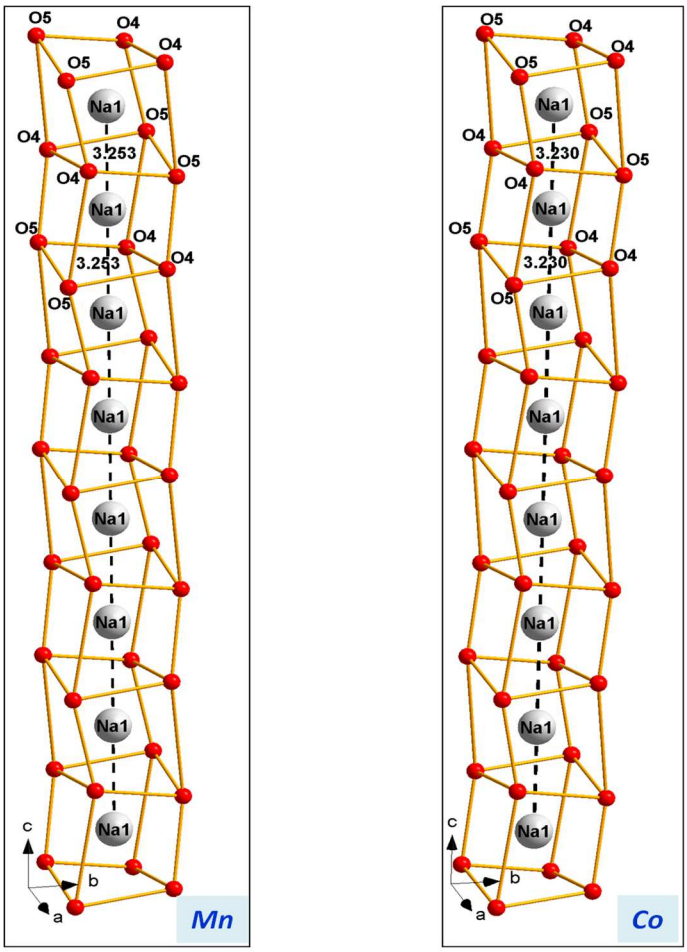

Figure 7. Comparison of tunnels occupied by sodium atoms Na1 in the structure of NMFP, (M = Mn and Co).

Thus, two adjacent parallelepipeds each containing a sodium atom Na1, at distances Na1-Na1 of 3.26 and 3.23 Å for $Na_2Mn_2Fe(PO_4)_3$ and $Na_2Co_2Fe(PO_4)_3$ compounds, respectively, as shown in **Figure 7**.

As indicated in the **Figure 8** below, the sodium atoms Na2 are located in the second type of tunnel, are arranged in zig-zag along $\vec{c}$ axis, with $Na2-\widehat{Na2}-Na2$ angles of 164.89 and 165.23 °, and Na2–Na2 distances of 3.28 and 3.26 Å for NMFP and NCFP, respectively. In these tunnels, the oxygen atoms O3 and O6 belonging to the different polyhedra MO6, FeO6 and PO4 of each tunnel, form pseudoparallelepipedic cavities O(3)O(6)O(3)O(6)─O(3)O(6)O(3)O(3), stacked along the $\vec{c}$ axis, with the Na^+ cations located in the center of each cavity in the particular 4e position.

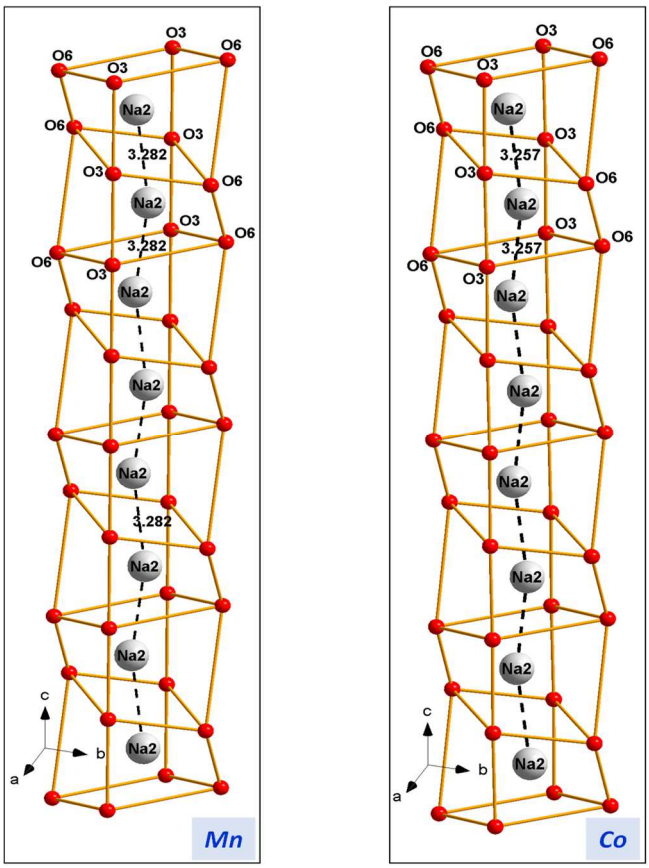

Figure 8. Comparison of tunnels occupied by sodium atoms Na2 in the structure of NMFP, (M = Mn and Co).

For the $Na_2Ni^{2+}{}_2Fe^{3+}(PO_4)_3$ (NNFP) compound, the crystal structure determination was carried out in orthorhombic symmetry with the centrosymmetric space group *Imma*, taking as the starting structural model, that described in the previous structural studies on the $Na_2Ni^{2+}{}_2Fe^{3+}(PO_4)_3$ phases with M = Fe and Cr [50,51]. Thus, to begin the structural refinement, the different atoms were placed in the following crystallographic sites: the Na in the 4e and 4b sites, the transition metals Ni and Fe in the 8g and 4a sites, P in atomic positions 8g and 4e and finally the four oxygen atoms in two positions 16j, as well as the 8h and 8i sites.

At the start of structural refinement, the metal atoms Ni, Fe were distributed over the two sites 8g and 4a, respecting their stoichiometries in the formula $Na_2Ni^{2+}{}_2Fe^{3+}(PO_4)_3$, with the occupancy rates of (75% Ni, 25% Fe) in site 8g and (50% Ni, 50% Fe) in site 4a. After several cycles of refinement, freeing all the parameters, only the structural model with a total occupation of the crystallographic sites 4a (1/2, 1/2, 1/2) by the Fe atoms and 8g (1/4, y , 1/4) by the Ni atoms, gave the best reliability factors, confirming an ordered distribution of the Ni and Fe atoms in the NNFP structure. The refinement of the structural and profile parameters was continued until the various reliability factors converged. The diffraction diagrams presented in **Figure 3**, attest to the good agreement obtained between the observed and calculated diffractograms, illustrated by the difference

between them. The low values of the reliability factors obtained at the end of the refinements attest also to the quality of the structural determination.

Thus, in the orthorhombic NNFP compound, the structure can be described from an assembly of FeO_6, NiO_6 and PO_4 polyhedra, where the crystal structure can be described as the association of two types of anionic entities, presented in **Figure 9 :** (i) a tetramer of nickel phosphates $[Ni_2P_2O_4]^{14-}$, created by the association of a dimer of Ni_2O_{10} obtained by pooling an O4─O4 edge between two NiO_6 octahedra; and two tetrahedra of $P(1)O_4$ sharing opposite O2–O2 edges of the Ni_2O_{10} dimer; **Figure 9a** (ii) an infinite chain $^1_\infty[FePO_8]^{8-}$ parallel to direction [010], obtained by the association of octahedron FeO_6 and tetrahedra $P(2)O_4$, connected to each other by the pooling of two opposite vertices O3 **Figure 9b**. The two anionic entities, the infinite chains $^1_\infty[FePO_8]^{8-}$ and the adjacent $[Ni_2P_2O_{14}]^{14-}$ tetramers, are connected in an alternating manner in the [100] direction, by the pooling of O2, O4 and O2 vertices, to form an infinite layer $^2_\infty[Ni_2Fe(PO_4)_3]^{2-}$ parallel to the plane (110), presented in **Figure 9b**.

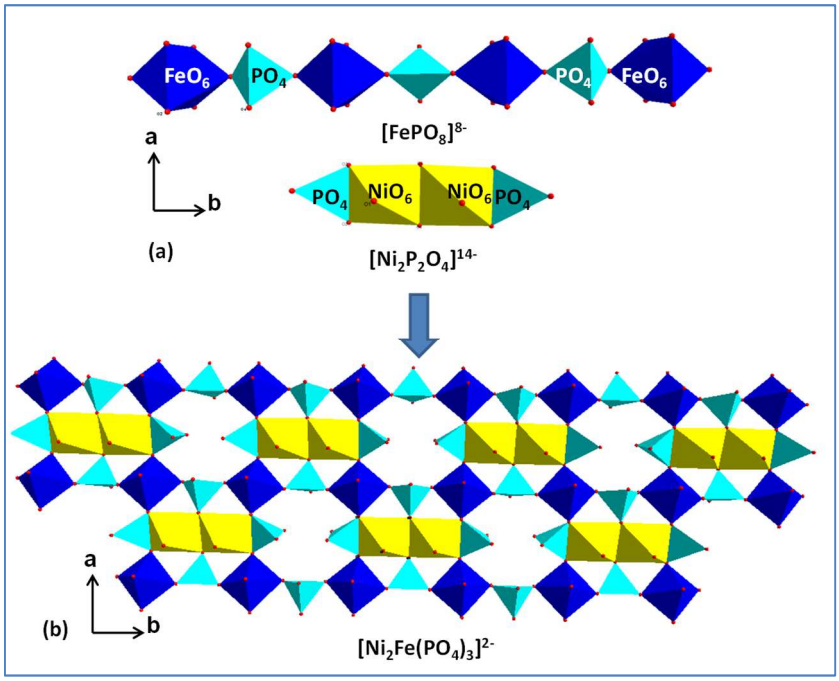

Figure 9. View of infinite layer $^2_\infty[Ni_2Fe(PO_4)_3]^{2-}$ (b), obtained by association infinite chain $^1_\infty[FePO_8]^{8-}$and $[Ni_2P_2O_4]^{14-}$ nickel phosphates tetramer (a)

The crystal structure of orthorhombic compound $Na_2Ni^{2+}{}_2Fe^{3+}(PO_4)_3$ is obtained by a stacking along the axis [100], of infinite layers $^2_\infty[Ni_2Fe(PO_4)_3]^{2-}$, connected to each other by the pooling of oxygen atoms O1 between two consecutive layers; to form a three-dimensional anionic framework releasing two different channels : Narrow rectangular tunnels along the [100] axis, **Figure 10a**, and large hexagonal tunnels along [010] direction, **Figure 10b**. The Na^+ monovalent cations are located inside these tunnels and participate in the cohesion of the structure, where the wide hexagonal tunnels are occupied by both Na1 and Na2 atoms, while the narrow rectangular channels are populated only by Na1 sodium atoms, as indicated in the **Figure 10**.

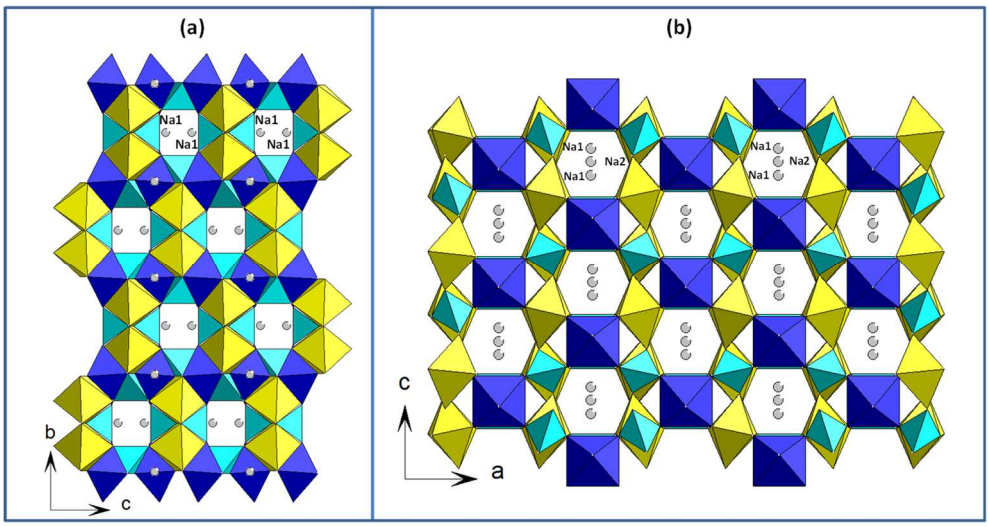

Figure 10. Comparison of tunnels occupied by sodium in $Na_2[Ni_2Fe(PO_4)_3]$ structure.

As shown in **Figure 11a**, inside each rectangular tunnel formed only by two types of oxygen atoms, O1 and O3, solely sodium atoms Na1 are present in these tunnels, located in deformed polyhedra, formed by 10 oxygen atoms (8xO1 and 2xO3) and linked to each other by O1─O1─O1─O1 rectangular faces, with Na-Na distances of the order 5.51Å and Na1 atoms very close to the walls of the tunnels inside a rectangle formed by four O1 oxygen, of width 3.104 Å and length 4.384 Å.

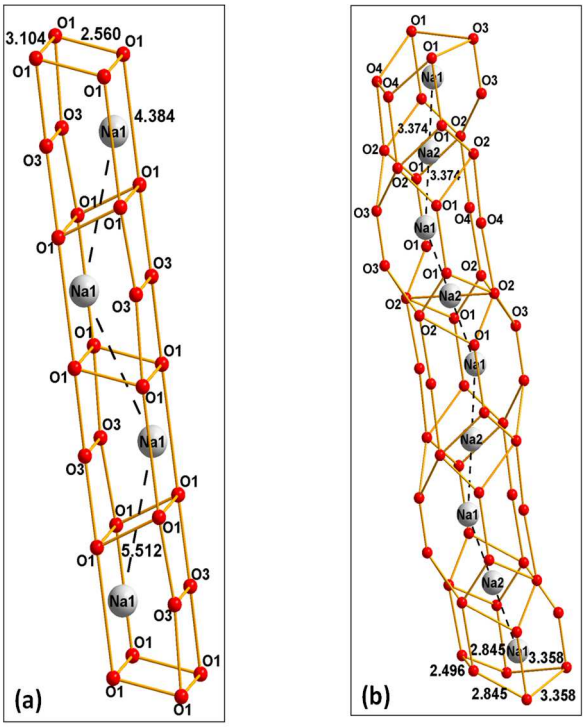

Figure 11. Sodium occupation of hexagonal and rectangular tunnels in the orthorhombic structure of NNFP

Regarding the large hexagonal tunnels oriented along the $\vec{b}$ axis and occupied alternately by the sodium atoms Na1 and Na2, the distances Na1─Na2 between two neighboring sodium atoms are much greater short than in rectangular tunnels, with distances of 3.371 Å, **Figure 11b**. This cationic density in the hexagonal tunnels will therefore promote the mobility of the alkaline Na^+ cations, that

will preferably occur through these tunnels. It is also worth noting the difference between the monodimensional channels observed in the two types of structures, with almost linear tunnels in the monoclinic symmetry for the NMFP MCFP compounds. While in the orthorhombic network for NNFP the tunnels are zig-zag shaped. To evaluate the Na^+ cation mobility in both structures, electrical conductivity measurements using impedance complex method have been performed for all compounds. Given the tunnel structures of the three compounds, they can be also potentially usable as positive electrodes in sodium-ions type batteries. Therefore, it is important to study the powders morphology, because a small particle-size is favorable to the process of intercalation in the primary particles by reducing the length of the Na-ion diffusion path.

3.2. Thermal analysis

TGA/DTA thermal analyzes of all compounds were performed in two steps. In first time, the study of the thermal evolution of the precursors obtained just after autocombustion synthesis, in the range of room temperature to 800°C, to follow their degradation and determine the crystallisation and synthesis temperatures of each compound. The second thermal analyses have been done after synthesis of different samples, to determine melting points and the sintering temperatures of pellets used for electrical measurements, as indicated in **Figure 12** and **table 6**.

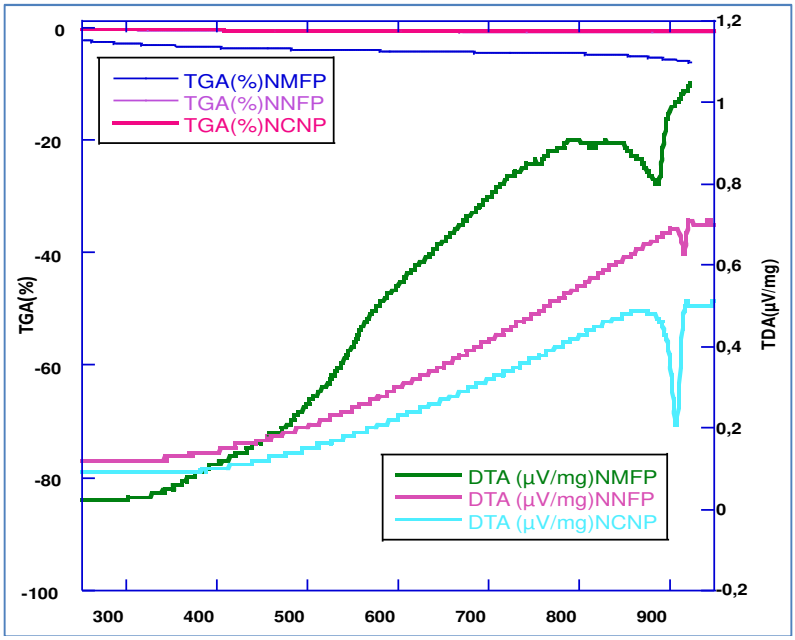

Figure 12. Thermal analyzes of NMFP, NNFP and NCFP phases

Table 6. Thermal, mechanical and electrical properties of $Na_2M^{2+}{}_2Fe^{3+}(PO_4)_3$, M = Mn, Co and Ni

	Crystallization temperature (°C)	**Melting point**	**Pelettes sintering temperature (°C)**	**Theoretical density(g/cm^3)**	**Pellets density (%)**
$Na_2Mn_2Fe(PO_4)_3$	~ 540	890	790	3.337	96
$Na_2Co_2Fe(PO_4)_3$	~ 570	900	790	3.543	97
$Na_2Ni_2Fe(PO_4)_3$	~ 640	920	820	3.757	90

3.3. Morphological properties

Figures 13 a, b and c show the SEM images of the three powders, respectively, where **Figure 13a** reveals that the particle size of $Na_2Mn^{2+}{}_2Fe^{3+}(PO_4)_3$ is the smallest of the three samples and ranged from 0.2 to 1 µm. While in the $Na_2Co^{2+}{}_2Fe^{3+}(PO_4)_3$ sample, the crystallites of prismatic shape, have a slightly larger particle size, ranging between 0.5 and 2.5 µm as indicated in the **Figure 13b**. For the compound of orthorhombic structure $Na_2Ni_2Fe(PO_4)_3$, as presented in Fig. 12c, the particles are of homogeneous morphology with regular micrometric sizes and a particle size range of approximately 0.5 to 3 µm. Thus, by using the J-image software to calculate the average particle size in the different samples, one obtains average sizes of the order of 0.5, 1.0, and 1.3 µm for the compounds NMFP, NCFP and NNFP, respectively.

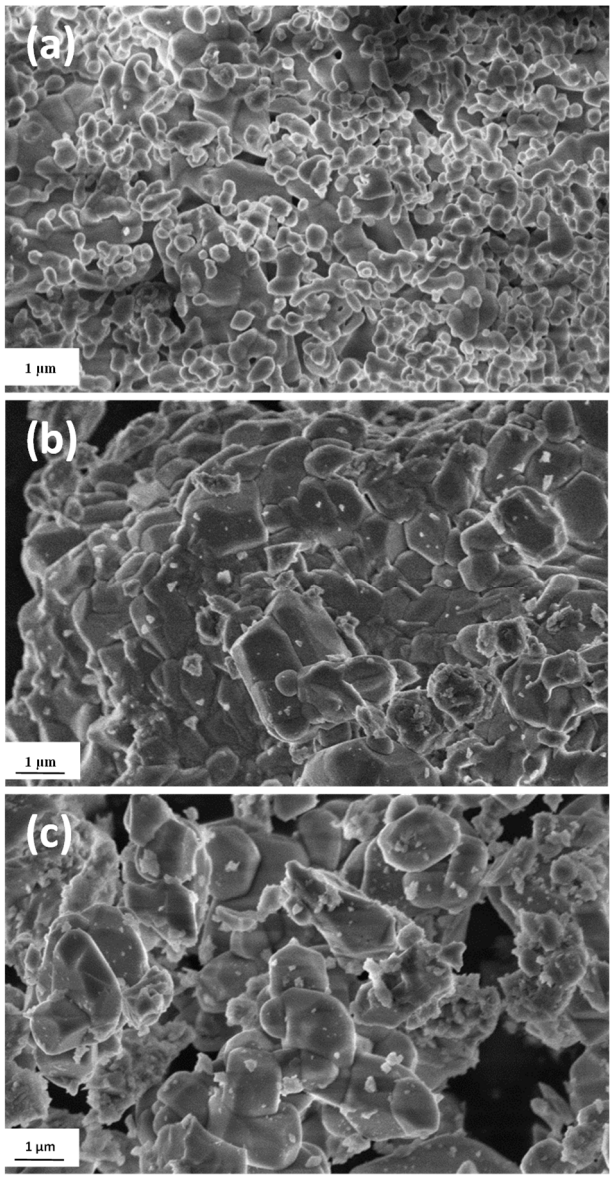

Figure 13. SEM images of compounds (a) NMFP, (b) NCFP and (c) NNFP prepared by autocombustion

While, using powder X-ray diffraction data of the three compounds, the profile and lattice parameter refinements with Thompson-Cox-Hasting profile option, allowed to obtain the real mean particle size

about (D_{Mn} = 81 nm, D_{Co} = 92 nm and D_{Ni} = 83 nm) with stress parameters of (η_{Mn} = 0.10%, η_{Co} = 0.09% and η_{Ni} = 0.11%), for NMFP, NCFP and NNFP compounds, respectively. From an electrochemical view point , this the observed morphplogies, with primary particules sizes varying from 81 to 92 nm, is suitable because it allows facile insertion/ deinsertion of soduin ions during the the reduction/oxidation of transition metal atoms.

With the X-ray diffraction refinement no impurities were detected as also confirmed by SEM analyzes using energy dispersive X-ray spectroscopy (EDX) analysis, which allowed us to probe the particles of each sample to confirm the homoginity of the latter, with the presence of all the elements corresponding to the appropriate chemical formula for each compound, **Figure 14 (a, b, c)**.

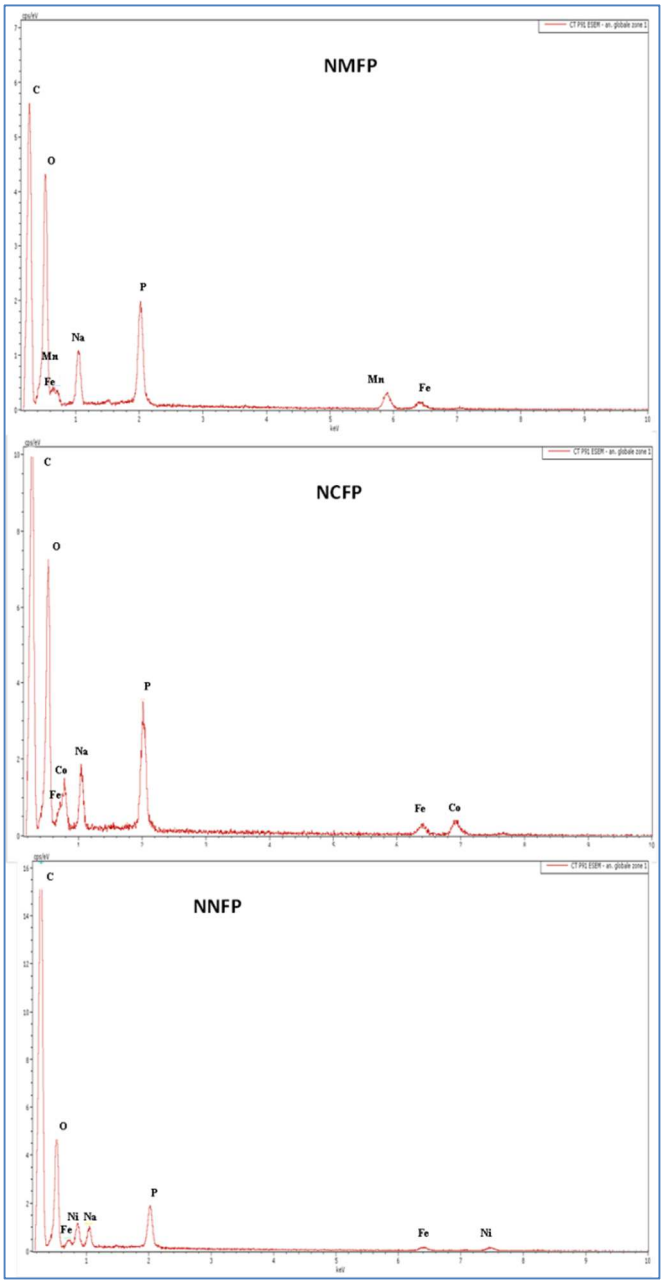

Figure 14. Energy dispersive X-ray spectroscopy (EDX) analysis of (a) NMFP, (b) NCFP and (c) NNFP.

Thus, EDX examination of each $Na_2M_2Fe(PO_4)_3$ sample confirms the presence of Na, M, Fe and P elements and also reveals uniform distribution of these elements throughout the surface of each studied sample. It is worth noting also that the EDX results give the atomic ratio of (Fe:M) of about 1:2.04, 1:2.08, 1:1.97 for M = Mn, Co and Ni, respectively, which is close to the theoretical value (1:2) in $Na_2M^{2+}{}_2Fe^{3+}(PO_4)_3$

3.4. Electrical and Electrochemical properties

- *Electrical conductivity properties*

Given the melting points obtained during the thermal study of the various compounds, the pellets used for the electrical conductivity measurements were sintered in air at 790°C for NMFP and NCFP, while the NNFP pellets have been sintered in air at 820°C. Thus, Table 6 indicates the obtained densities of the sintered pellets of different compounds. The ionic conductivity measurements were conducted by using impedance spectroscopy technique to evince the mobility of Na^+ cations in the tunnels of different structures. Thus, the **Figure 15** presents the typical complex impedance spectra for different pellets as solid electrolytes at 400°C. It is observed that the total impedance of the orthorhombic compound NNFP is much lower than those of monoclinic compounds NMFP and NCFP. This high electrical conductivity of NNFP compound clearly shows the effect of network symmetry on the mobility of Na^+ cations in the tunnels.

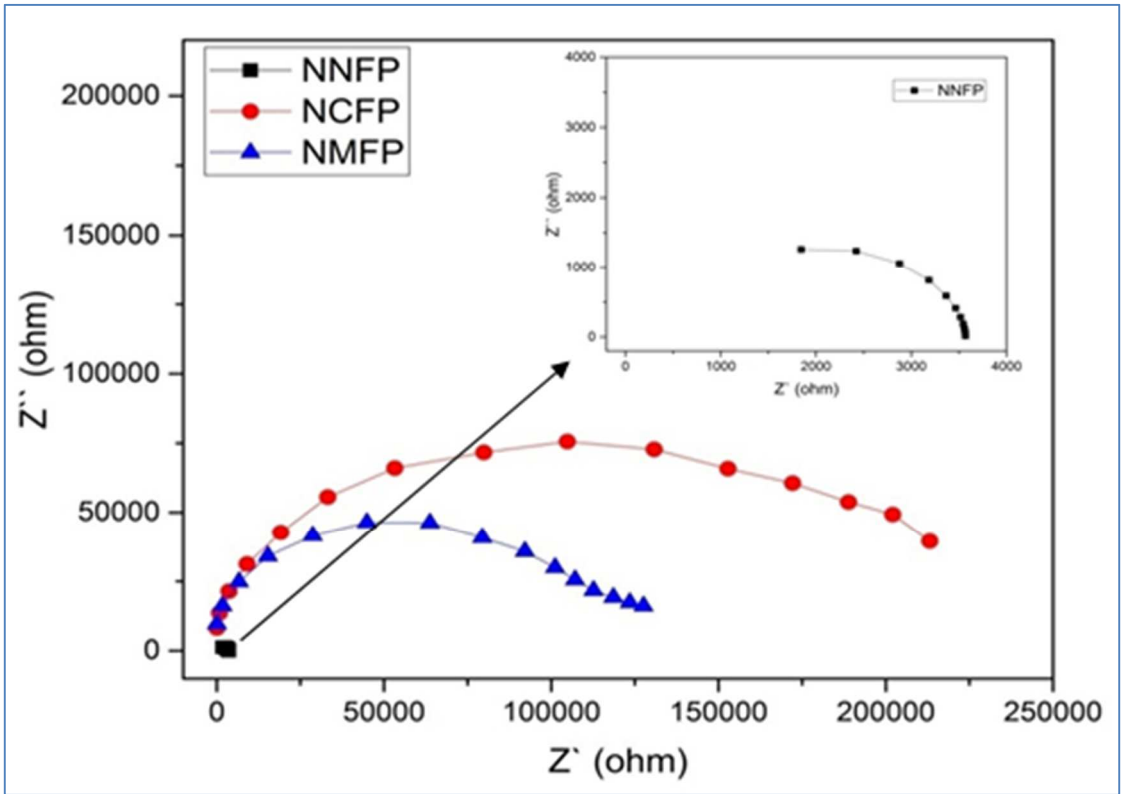

Figure 15. Complex impedance spectra of NMFP, NCFP and NNFP samples at 400°C. Inset graph is the magnified complex impedance plot of NNFP.

Zview software **[56]** was used to fit Nyquist plots of each compound. It can be noted that in high frequency domain, the impedance diagrams show only one typical semicircle arc. Thus, for the three fist temperature, two equivalent circuits containing a resistor R connected in parallel with a constant phase element CPE have been used to adjust the impedance diagrams. The latter contribution is an empirical impedance function of the type: $Z_{(CPE)} = \frac{1}{A(j\omega)^p}$; (-1 ≤ p≤1), where A is a pseudo capacitance obtained from CPE. However, At higher temperatures, the impedance spectra are shifted from their origin, and An equivalent circuit collected a resistor R connected in parallel with a constant phase element CPE was used to fit impedance spectra. Thus,an example of extracted and calculated values of different electric parameters for NNFP, at different temperatures, are illustrated in Table 7.

Table 7. Electrical parameters of NNFP obtained from equivalent circuits at 192≤ T(°C) ≤401, refined using Z-view software and σ_{dc} conductivity

T(°C)	R1 (Ω)	A1 (10^{-11} Fs^{p-1})	P1	C1 (10^{-12}F)	R2 (Ω)	A2 (10^{-11} Fs^{p-1})	P2	C2 (10^{-12}F)	σ_{dc} ($S.cm^{-1}$)
192	35743	1.90	0.9337	2.7229	421170	5.84	0.8355	0.4106	$2.918\ 10^{-6}$
241	34736	8.95	0.8195	0.3918	81433	5.35	0.8838	0.8285	$1.1478\ 10^{-5}$
293	20548	5.14	0,8867	1.9114	13344	0.38	0.7513	0.2028	$3.934\ 10^{-5}$
343	11829	3.98	0.8689	8.0676	731				$1.062\ 10^{-4}$
347	10407	2.58	0.8920	1.0442	764				$1.194\ 10^{-4}$
349	10220	3.12	0.8827	9.5940	786				$1.212\ 10^{-4}$
401	3852	1.80	0.9316	2.4218	912				$2.799\ 10^{-4}$

Linear Arrhenius plot of $\log(\sigma_{dc}T$ ($\Omega^{-1}.cm^{-1}.K$)) vs. 1000 /T (K^{-1}) given in **Figure 16**, confirm the best electrical conductivity of the orthorhombic $Na_2Ni^{2+}{}_2Fe^{3+}(PO_4)_3$ compound in all thermal domain, with activation energies of 0.63, 0.65 and 0.75eV for NNFP, NCFP and NMFP compounds, respectively. The electrical conductivity deceasing between orthorhombic and monoclic symmetry can be linked to channels dimension present in both structures. In fact, the decrease in the size of tunels in the crystaline framework, causes lowering in the mobility of Na ions in the structure.Therefore, it is found that NNFP has a best electrical conductivity with a lowest value of activation energy of about 0.63 eV, as a result of large size of open channels in orthorhombic symmetry. Thus, the activation energy value of Na ion diffusion, observed in the orthorhombic compound NNFP (0.63 eV) , confirms that the migration path with the lowest activation energy corresponds well to mono-dimensional tunnels with a zigzag pattern, as observed in Figue 11.

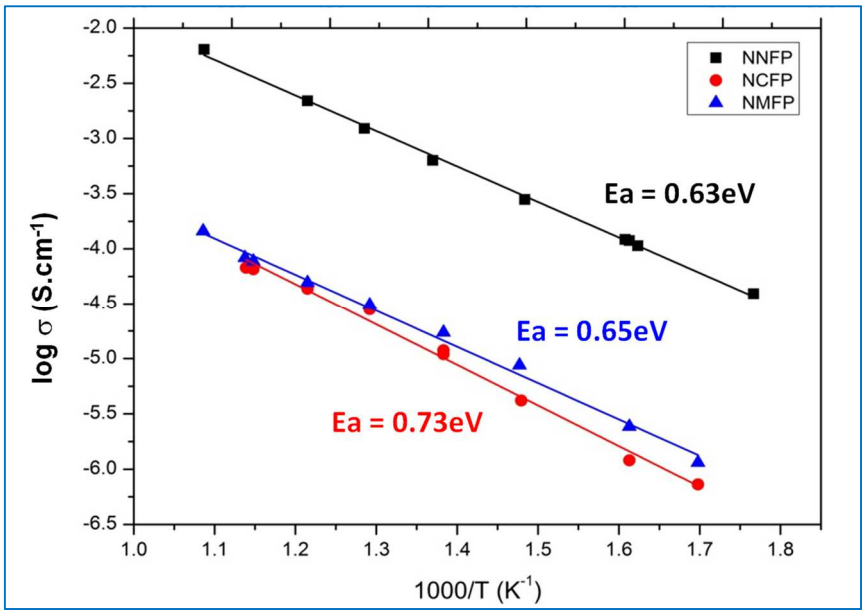

Figure 16. Arrhenius plots of ionic conductivity of bulk samples NMFP, NCFP and NNFP.

As the ionic radius of divalent transition metal ions M^{2+} (M = Co, Mn, and Ni) in an octahedral environment is following the orderer of $R_{Co}^{2+} < R_{Mn}^{2+} < R_{Ni}^{2+}$ (R_{Co}^{2+} = 0,79Å, R_{Mn}^{2+} = 0,81Å et R_{Ni}^{2+} = 0,83 Å), [62, 63], the average distance <Na─O> in the tunnels formed by these octahedra increase with the radii of the M^{2+} cations, inducing lower $<Na─O>_{Co2+}$ distances and strongest Na─O chemical bonds in the tunnels of the $Na_2Co_2Fe(PO_4)_3$ compounds, which results in a greater activation energy of 0.73 eV observed for cobalt compound.

- *Electrochemical properties*

To investigate the effects, both of the (monoclinichor/orthorhombic) crystal structure symmetry and of M^{2+} divalent transition metal ion substitution, on the electrochemical performance in the $Na_2M^{2+}{}_2Fe^{3+}(PO_4)$ compounds (M = Co, Mn, Ni) used as positive electrode materials in Na-ions batteries, preliminary electrochemical measurements were performed. Thus, electrochemical tests of the three samples as cathode materials were carried out by galvanostatic cycling, with sodium metal as negative electrodes.

In order to deduce the kinetic effect and approach a thermodynamic equilibrium of sodium exchange during the first electrochemical measurements, low cycling rates have been performed with Charge/discharge rates of C/100, in a potential window of 1.5 to 4.2 V, as indicated in **Figure 17**.

The electrochemical charge/discharge measurements presented in **Figure 17**, show that the three electrochemical cells folow similar cycling profiles, with a better performances obtained for manganese material NMFP. Thus, during the first discharge cycle of NMFP cell about 0.85 Na^+ ions per formula unit could be intercalated and about 0.64 Na^+ ion per formula unit could be extracted from the structure at the following charge. However, the cobalt material NCFP exhibits the lowest Na^+ ions exchange, of about 0.56 and 0.34 Na^+ ion during the Na extraction and insertion processes,

respectively. Whereas, the orthothombic compound NNFP exhibits intermediate values with an insertion of 0.66 and a deinsetion of 0.44 Na^+ ion during charge and discharge steps, respectively. Alternatively, the specific charge capacity of NMFP, NNFP and NCFP cathode materials are about 94.2, 84.4 and 66 mAh/g corresponding to 75.5, 75 and 57.3% of coloumbic efficiency, respectively. This preliminary study clearly shows that the powder morphology plays an important role in the electrochemical process. Thus, as it has been observed for NMFP, a material with a smaller grain size promotes the mobility of Na^+ cations in the primary particles, by reducing the length of the ion diffusion path in the electrode material, [41, 43, 40, 50]. Such a morphology is also favorable to better impregnation of the electrolyte and therefore better ionic percolation.

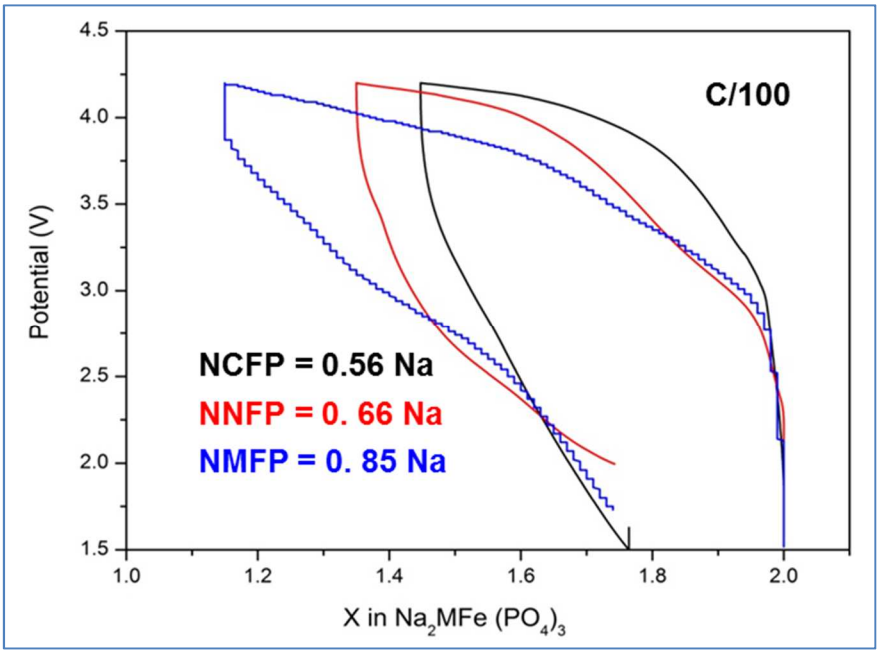

Figure 17. charge/discharge profiles of $Na_2M^{2+}{}_2Fe^{3+}(PO_4)$ cathodes at a rate of C/100.

By comparing the results of orthorhombic NNFP and monoclinic NCFP compounds, having same particles sizes, one observe the crystal structure effect , with the best electrochemical recycling for the NNFP compound of orthorhombic symmetry.

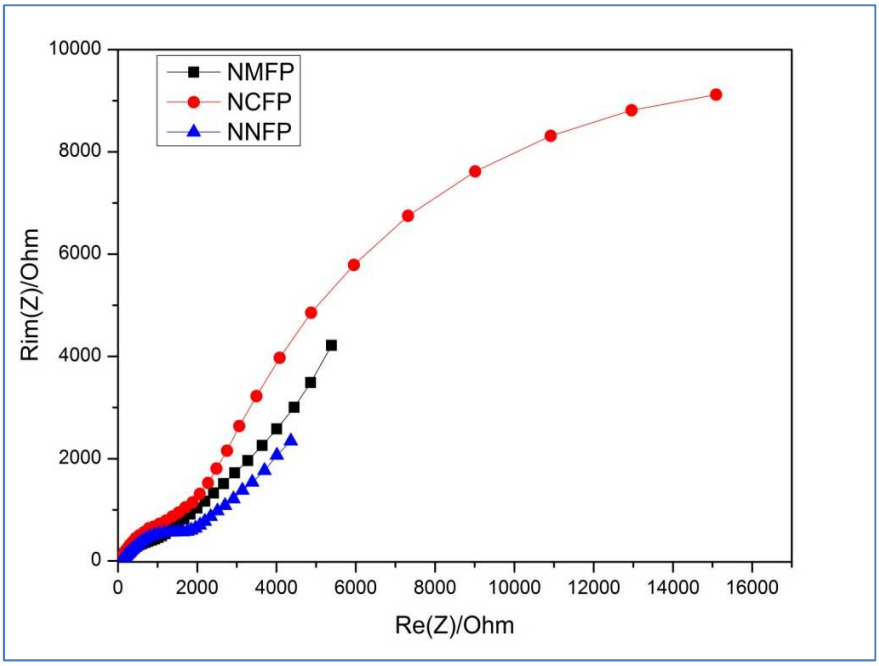

Figure 18. the Nyquist plot of both sample electrodes after the first cycle

Figure 18 illustrates the typical EIS plots of the three cycled batteries after the first cycle to further confirm and support the charge/discharge tests. Eventually, the NMFP cell revealed the minimum resistance for the bulk (Rs), for charge transfer (R_{ct}) and for Na^+ ion diffusion as well. On the contrast, the battery with NCFP cathode showed higher Rs and R_{ct} along with poor Na^+ ion diffusion between the electrolyte and electrode surface.

4. Conclusions

The variations of structural, morphological, electrical and electrochemical properties of Alluaudite Phases $Na_2M^{2+}{}_2Fe^{3+}(PO_4)_3$ (M = Mn, Co and Ni) of powdred samples have been investivated. The three compounds were synthesised by autocombustion route and its crystal structures were determined using pouder X-ray diffraction data.The cobalt and manganese phases crystallise in monoclinic symmetry, while nickel compound adopts an orthorhombic crystal structure. In both crystalline symmetries the crystal structure form a three-dimensional anionic framework releasing different channels occupied monovalent cations Na^+. Thus, sodium atoms are located within the 3D-frameworks of octahedra and tetraeadra sharing corners and/or edges with small square and large hexagonal channels along [100] and [010] respectively in orthorhombic structure, and with two different tunnels according [001] direction in monoclinic structure. The presence of sodium cations in the tunnels confer them better mobility and good electrical and electrochemical properties. The three materials $Na_2M^{2+}{}_2Fe^{3+}(PO_4)_3$ (M = Mn, Co and Ni) have also demonstrated their potential for use as cathode material with specific charge capacities 94.2, 84.4 and 66 mAh/g, respectively.

References

[1] Crabtree, G. Perspective: the energy-storage revolution, *Nature 526, S92 (2015).*

[2] Z. Jian, W. Han, X. Lu, H. Yang, Y.-S. Hu, J. Zhou,Z.Zhou, J. Li, W. Chen, D. Chen, L. Chen, Superior Electrochemical Performance and Storage Mechanism of $Na_3V_2(PO_4)_3$ Cathode for Room-Temperature Sodium-Ion Batteries, *Adv. Energy Mater. 2013, **3**, 156 - 160.*

[3] Obama, B. The irreversible momentum of clean energy, *Science 355, 126–129 (2017).*

[4] Yuanli Ding, Zachary P. Cano, Aiping Yu, Jun Lu & Zhongwei Chen, Automotive Li-Ion Batteries: Current Status and Future Perspectives, *Electrochemical Energy Reviews volume **2**, 1 - 28 (2019)*

[5] Kubota, K.; Kumakura, S.; Yoda, Y.; Kuroki, K.; Komaba, S., Electrochemistry and Solid-State Chemistry of NaMeO2 (Me = 3d Transition Metals), *Adv. Energy Mater. 2018, **8**, 1703415*.

[6] Vaalma, C.; Buchholz, D.; Weil, M.; Passerini, S., A cost and resource analysis of sodium-ion batteries, *Nat. Rev. Mater. 2018, **3**, 18013.*

[7] Jin, Y.; Xu, Y.; Le, P. M. L.; Vo, T. D.; Zhou, Q.; Qi, X.; Engelhard, M. H.; Matthews, B. E.; Jia, H.; Nie, Z.; Niu, C.; Wang, C.; Hu, Y.; Pan, H.; Zhang, J.-G. , Highly Reversible Sodium Ion Batteries Enabled by Stable Electrolyte-Electrode Interphases, *ACS Energy Lett. 2020, **5**, 3212−3220*

[8] Song, J.; Wang, K.; Zheng, J.; Engelhard, M. H.; Xiao, B.; Hu, E.; Zhu, Z.; Wang, C.; Sui, M.; Lin, Y.; Reed, D.; Sprenkle, V. L.; Yan, P.; Li, X., Controlling Surface Phase Transition and Chemical Reactivity of O3-Layered Metal Oxide Cathodes for High-Performance Na-Ion Batteries, *ACS Energy Lett. 2020, **5 (6)**, 1718−1725.*

[9] Slater, M. D.; Kim, D.; Lee, E.; Johnson, C. S. Adv. Funct. Mater. 2013, 23, 947.

[10] Komaba, S.; Murata, W.; Ishikawa, T.; Yabuuchi, N.; Ozeki, T.; Nakayama, T.; Ogata, A.; Gotoh, K.; Fujiwara, K. Electrochemical Na Insertion and Solid Electrolyte Interphase for Hard-Carbon Electrodes and Application to Na-Ion Batteries, Adv. Funct. Mater. 2011, 21, 3859.

[11] Kim, S. W.; Seo, D. H.; Ma, X. H.; Ceder, G.; Kang, K. Electrode Materials for Rechargeable Sodium-Ion Batteries: Potential Alternatives to Current Lithium-Ion Batteries, Adv. Energy Mater. 2012, 2, 710-721.

[12] N. Yabuuchi, M. Kajiyama, J. Iwatate, H. Nishikawa, S. Hitomi, R. Okuyama, R. Usui, Y. Yamada, and S. Komaba. P2-type Nax [Fe1/2 Mn1/2[O2 made from earth-abundant elements for rechargeable Na-batteries, Nat. Mater. 2012, 11, 512-517.

[13]. R. Berthelot, D. Carlier, and C. Delmas. Electrochemical investigation of the P2–NaxCoO2 phase diagram, Nat. Mater. 2011, 10, 74-80.

[14]. Y. S. Wang, R. J. Xiao, Y. S. Hu, M. Avdeev, and L. Q. Chen. P2-$Na_{0.6}[Cr_{0.6}Ti_{0.4}]O_2$ cation-disordered electrodefor high-rate symmetric rechargeable sodium-ionbatteries, Nat. Commun. 2015, 6, 6954-6963

[15]. K. Kubota, N. Yabuuchi, H. Yoshida,M. Dahbi, and S. Komaba. Layered oxides as positive electrode materials for Na-ion batteries, MRS Bull. 2014, 39, 416-422.

[16]. J. F. Whitacre, A. Tevar, and S. Sharma. Na4Mn9O18 as a positive electrode material for an aqueous electrolyte sodium-ion energy storage device, Electrochem. Commun. 2010, 12(3), 463-466.

[17]. Y. H. Liao, K. S. Park, P. H. Xiao, G. Henkelman, W. S. Li, and J. B. Goodenough. Sodium Intercalation Behavior of Layered NaxNbS2 ($0 \leq x \leq 1$), Chem. Mater. 2013, 25(9), 1699-1705.

[18]. E. Lee, S. Sahgong, C. S. Johnson, and Y. Kim. Comparative electrochemical sodium insertion/extraction behavior in layered Na_xVS_2 and Na_xTiS_2, Electrochim. Acta. 2014, 143, 272-277.

[19]. I. Gocheva, M. Nishijima, T. Doi, S. Okada, J. Yamaki, and T. Nishida. Mechanochemical synthesis of NaMF3 (M = Fe, Mn, Ni) and their electrochemical properties as positive electrode materials for sodium batteries, J. Power Sources 2009, 187(1), 247-252.

[20]. C. L. Li, C. L. Yin, L. Gu, R. E. Dinnebier, X. K. Mu, P. A. van Aken, and J. Maier. An FeF3·0.5H2O Polytype: A Microporous Framework Compound with Intersecting Tunnels for Li and Na Batteries, J. Am. Chem. Soc. 2013, 135(31), 11425-11428.

[21]. C. L. Li, C. L. Yin, X.. Mu, and J. Maier. Top-Down Synthesis of Open Framework Fluoride for Lithium and Sodium Batteries, Chem. Mater. 2013, 25(6), 962-969.

[22]. Y. Kawabe, N. Yabuuchi, M. Kajiyama, N. Fukuhara, T. Inamasu, R. Okuyama, I. Nakai, and S. Komaba. Synthesis and electrode performance of carbon coated Na_2FePO_4F for rechargeable Na batteries, Electrochem. Commun. 2011, 13(11), 1225-1228.

[23]. Z. Jian, L. Zhao, H. Pan, Y. S. Hu, H. Li, W. Chen, and L. Chen. Carbon coated $Na_3V_2(PO_4)_3$ as novel electrode material for sodium ion batteries, Electrochem. Commun. 2012, 14(1), 86.-89

[24]. H. Kim, I. Park, D. H. Seo, S. Lee, S. W. Kim, W. J. Kwon, Y. U. Park, C. S. Kim, S. Jeon, and K. Kang. New iron-based mixed-polyanion cathodes for lithium and sodium rechargeable batteries: combined first principles calculations and experimental study, J. Am. Chem. Soc. 2012, 134(25), 10369-10372.

[25]. M. Nose, S. Shiotani, H. Nakayama, K. Nobuhara, S. Nakanishi, and H. Iba. $Na_4Co_{2.4}Mn_{0.3}Ni_{0.3}(PO_4)_2P_2O_7$: High potential and high capacity electrode material for sodium-ion batteries, Electrochem. Commun. 2013, 34(1), 266-269.

[26]. P. Moreau, D. Guyomard, J. Gaubicher, and F. Boucher. Structure and Stability of Sodium Intercalated Phases in Olivine FePO4, Chem. Mater. 2010, 22(14), 4126-4128.

[27]. S. M. Oh, S. T. Myung, J. Hassoun, B. Scrosati, and Y. K. Sun. Reversible NaFePO4 electrode for sodium secondary batteries, Electrochem. Commun. 2012, 22(1), 149-152.

[28]. P. Barpanda, G. Oyama, S.-i. Nishimura, S.-C. Chung, and A. Yamada. A 3.8-V earth-abundant sodium battery electrode, Nat. Commun. 2014, 5, 4358-4366.

[29]. P. Serras, V. Palomares, A. Goni, I. G. de Muro, P. Kubiak, L. Lezama, and T. Rojo. High voltage cathode materials for Na-ion batteries of general formula $Na_3V_2O_{2x}(PO_4)_2F_{3-2x}$, J. Mater. Chem. 2012, 22, 22301-22308.

[30]. Y. U. Park, D. H. Seo, H. S. Kwon, B. Kim, J. Kim, H. Kim, I. Kim, H. I. Yoo, and K. Kang. A new high-energy cathode for a Na-ion battery with ultrahigh stability, J. Am. Chem. Soc. 2013, 135(37), 13870–1387.

[31]. J. Lu, S. C. Chung, S. I. Nishimura, and A.Yamada. Phase Diagram of Olivine NaxFePO4 ($0 < x < 1$), Chem. Mater. 2013, 25(22), 4557–4565.

[32]. Y. Lu, L. Wang, J. Cheng, and J. B. Goodenough. Prussian blue: a new framework of electrode materials for sodium batteries, Chem. Commun. 2012, 48, 6544-6546.

[33]. H. W. Lee, R. Y. Wang, M. Pasta, S. W. Lee, N. Liu, and Y. Cui. Manganese hexacyanomanganate open framework as a high-capacity positive electrode material for sodium-ion batteries, Nat. Commun. 2014, 5. 5280-5286.

[34]. L. Wang, J. Song, R. M. Qiao, L. A. Wray, M. A. Hossain, Y. D. Chuang, W. L. Yang, Y. H. Lu, D. Evans, J. J. Lee, S. Vail, X. Zhao, M. Nishijima, S. Kakimoto, and J. B. Goodenough. Rhombohedral Prussian white as cathode for rechargeable sodium-ion batteries, J. Am. Chem. Soc. 2015, 137(7), 2548–2554.

[35]. R. R. Zhao, L. M. Zhu, Y. L. Cao, X. P. Ai, and H. X. Yang. An aniline-nitroaniline copolymer as a high capacity cathode for Na-ion batteries, Electrochem. Commun. 2012, 21, 36-38.

[36]] Q. Ni, Y. Bai, F. Wu, C. Wu, Polyanion-type electrode materials for sodium-ion batteries*, Adv. Sci. **4** (2017) 1600275.*

[37] Huang Xu Li, Kunjie Zhu, Peng-Fei Wang, Pei Liu, Lifang Jiao, *Chemical Society Reviews,* Polyanion-type cathode materials for sodium-ion batteries, 2020 **8**, 2342-2377.

[38] Xianghua Zhang, Xianhong Rui, Dong Chen,Huiteng Tan, Dan Yang, Shaoming Huang and Yan Yu, $Na_3V_2(PO_4)_3$: an advanced cathode for sodium-ion batteries, *Nanoscale, 2019,**11**, 2556-2576.*

[39] Mingzhe Chen, Weibo Hua, Jin Xiao, David Cortie, Xiaodong Guo, Enhui Wang, Qinfen Gu, Zhe Hu, Sylvio Indris, Xiao-Lin Wang, Shu-Lei Chou, and Shi-Xue Dou, Development and Investigation of a NASICON-Type High-Voltage Cathode Material for High-Power Sodium-Ion Batteries, *Angewandte Chemie, 2019, **59(6)**, 2470-2477*

[40] W. Huang, J. Zhou, B. Li, J. Ma, S. Tao, D. Xia, W. Chu and Z. Wu, Detailed investigation of $Na_{2.24}FePO_4CO_3$ as a cathode material for Na-ion batteries, *Sci. Rep., 2014, **4**, 4188, 1-8.*

[41] K. Trad, D. Carlier, L. Croguennec, A. Wattiaux, M. Ben Amara and C. Delmas, Structural Study of the $Li_{0.5}Na_{0.5}MnFe_2(PO_4)_3$ and $Li_{0.75}Na_{0.25}MnFe_2(PO_4)_3$ Alluaudite Phases and Their Electrochemical Properties As Positive Electrodes in Lithium Batteries, *Inorg. Chem.* 2010*,* 49*, 22, 10378-1038.*

[42] F. Hatert, The crystal chemistry of lithium in the alluaudite structure: a study of the $(Na_{1-x}Li_x)_{1.5}Mn_{1.5}Fe_{1.5}(PO_4)_3$solid solution (x= 0.5 to 1), *Mineralogy and Petrology, 2004, **81**, 1-3*.

[43] Khiem Trad, Dany Carlier, Laurence Croguennec, Alain Wattiaux, Mongi Ben Amara, and Claude Delmas, $NaMnFe_2(PO_4)_3$ Alluaudite Phase: Synthesis, Structure, and Electrochemical Properties As Positive Electrode in Lithium and Sodium Batteries, *Chem. Mater. 2010, **22**, 5554–5562*.

[44] R. Essehli, I. Belharouak, H. Ben Yahia, K. Maher, A. Abouimrane, B. Orayech, S. Calder, X. L. Zhou, Z. Zhoud and Y-K. Sune, Alluaudite $Na_2Co_2Fe(PO_4)_3$ as an electroactive material for sodium ion batteries, Dalton Trans., 2015, **44**, 7881–7886.

[45] G. Alhakmi, A. Assani, M. Saadi and L. El Ammari. Synthesis and crystal structure of two new phosphates with Alluaudite type structure: $(M, Mn)_3Fe(PO_4)_3$ (M= Ca , Cd), CMSS-2017, MATEC Web of Conferences, 2018, **149,** 01084- 01093**.**

[46] M. Hadouchi, A. Assani, M. Saadi, I. Saadoune, A. Lahmar, H. Bouyanfif, M. El Marssi, L. El Ammari. Synthesis, Crystal Structure and Properties of a New Phosphate, $Na_2Co_2Cr(PO_4)_3$, Journal of Inorganic and Organometallic Polymers and Materials 2018, **28(6),** 2854-2864.

[47] E. Benhsina, L. Hermouche, A. Assani, M. Saadi, N. Labjar, S. El Hajjaji, A. Lahmar, L. El Ammari, Synthesis, characterization, magnetic properties, and lead sensing based on a new alluaudite-like phosphate $Na_2Mn_2Cr(PO_4)_3$ Journal of Materials Science 2021, **56(3)**, 2163-2175

[48] Khalifa Souiwa, Madhu Chennabasappa, Rodolphe Decourt, Mongi Ben Amara, Mourad Hidouri and Olivier Toulemonde, Novel Mixed Cobalt/Chromium Phosphate $NaCoCr_2(PO_4)_3$ Showing Spin-Flop Transition, Inorg. Chem. 2015, **54**, 7345−7352

[49] F. Hatert, Crystal chemistry of the divalent cation in alluaudite-type phosphates: A structural and infrared spectral study of the $Na_{1.5}(Mn_{1-x}M^{2+}{}_x)_{1.5}Fe_{1.5}(PO_4)_3$ solid solutions (x = 0 to 1, M^{2+} = Cd^{2+}, Zn^{2+}), Journal of Solid State Chemistry 2008, **181**, 1258– 1272.

[50] R. Essehli, I. Belharouak, H. Ben Yahia, R. Chamoun, B. Orayech, B. El Bali, K. Bouziane, X. L. Zhou, Z. Zhou, α-$Na_2Ni_2Fe(PO_4)_3$: a dual positive/negative electrode material for sodium ion batteries, Dalton Trans.,2015, **44**, 4526–4532.

[51] H. BenYahia, R.Essehli, M.Avdeev, J-B.Park, Y-K.Sun, M.A.Al-Maadeed, I. Belharouak, Neutron diffraction studies of the Na-ion battery electrode materials $NaCoCr_2(PO_4)_3$, $NaNiCr_2(PO_4)_3$, and $Na_2Ni_2Cr(PO4)_3$, Journal of Solid State Chemistry 2016, **238**, 103–108

[52] D. Harbaoui, M. M. S.; Sanad, C. Rossignol, E. K. Hlil, N. Amdouni, S. Obbade. Synthesis and Structural, Electrical, and Magnetic Properties of New Iron–Aluminum Alluaudite Phases β-$Na_2Ni_2M(PO_4)_3$ (M = Fe and Al). Inorganic Chemistry 2017, **56(21)** 13051-13061.

[53] (18) Moore, P. B. Crystal chemistry of the alluaudite structure type: contribution to the paragenesis of pegmatitic phosphate giant crystals. Am. Mineral. 1971, **56**, 1955–1975.

[54] Karegeya, C.; Mahmoud, A.; Vertruyen, B.; Hatert, F.; Hermann, R. P.; Cloots, R.; Boschini, F. One-step hydrothermal synthesis and electrochemical performance of sodium-manganese-iron phosphate as cathode material for Li-ion batteries. J. Solid State Chem. 2017, **253**, 389–397.

[55] Oyama, G.; Kiuchi, H.; Chung, S. C.; Harada, Y.; Yamada, A. Combined experimental and computational analyses on the electronic structure of alluaudite-type sodium iron sulfate. J. Phys. Chem. 2016, **C120**, 23323–23328.

[56] Hatert, F., Fransolet, A.-M., Maresch,W.V.: The stability of primary alluaudites in granitic pegmatites: an experimental investigation of the $Na_2(Mn_{2-2x}Fe_{1+2x})(PO_4)_3$ system. Contrib. Mineral. Petrol. 2006, **152**, 399–419

[57]. Khmiyas, J.,Assani, A., Saadi, M., ElAmmari, L.: Crystal structure of a sodium, zinc and iron(III)-based non-stoichiometric phosphate with an alluaudite-like structure: $Na_{1.67}Zn_{1.67}Fe_{1.33}(PO_4)_3$. Acta Crystallogr. Sect. E Crystallogr. Commun. 2015, **71**, 690–692

[58] Rietveld, H. M. Line profiles of neutron powder-diffraction peaks for structure refinement. Acta Crystallogr. 1967, **22(1)**, 151-152.

[59] Rietveld, H. M. **A** profile refinement method for nuclear and magnetic structures,J. Appl. Crystallogr. **2** (1969) 65-71.

[60] Rodriguez-Carvajal J. FULLPROF 2011: A graphic tool for powder diffraction. Version January 2011.

[61] D. Johnson, "Zview version 3.1c" Scribner Associates. Inc. 1990-2007.

[62] Shannon, R. D.; Prewitt, C. T. Effective ionic radii in oxide and fluorides. Acta Crystallogr., Sect. B: Struct. Crystallogr. Cryst. Chem. 1969, **B25**, 925-945.

[63] Shannon, R. D. Revised effective ionic radii and systematic studies of interatomic distances in halides and chalcogenides. Acta Crystallogr., Sect. A: Cryst. Phys., Differ., Their. Gen. Crystallogr. 1976, **A32**, 751-767.

Polyanionic Phosphates : $Na_2M^{II}{}_2Fe^{III}(PO_4)_3$ with M^{II} = Co, Ni, Mn

Transition metal effect

Tow polymorphic crystal structures

$Na_2 (Co, Mn)^{II}{}_2Fe^{III}(PO_4)_3$

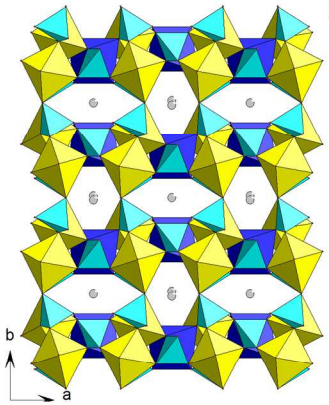

Deformed monoclinic symmetry

$Na_2Ni^{II}{}_2Fe^{III}(PO_4)_3$

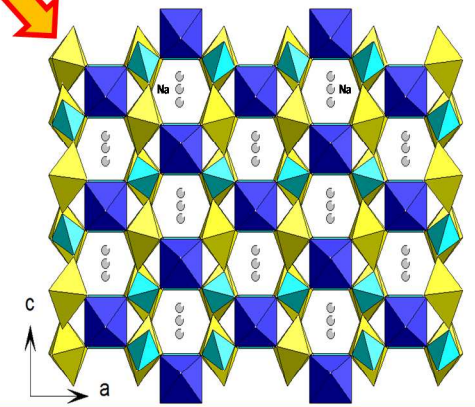

Symmetric orthorhombic symmetry